Student Conference Proceedings
Vol 2, No 1, 2026, Article ID 2613, 4 Pages

Student Conference Lübeck

Proceedings Article

Automated Reference Arm for Online Surface Tracking in Optical Coherence Tomography

Diana Mohammed [a,*] · Simon Lotz [b] · Robert Huber [b,*]

[a] Study program Biomedical Engineering, Luebeck University of Applied Sciences, Lübeck, Germany
[b] Institute of Biomedical Optics, Universität zu Lübeck, Lübeck, Germany
*Corresponding author, email: diana.rasheed.abdulqader.mohammed@stud.th-luebeck.de; robert.huber@uni-luebeck.de

Received 27 April 2026; Accepted 15 October 2026; Published online 27 October 2026

© 2026 Mohammed *et al.*; licensee Infinite Science Publishing
This is an Open Access article distributed under the terms of the Creative Commons Attribution License (http://creativecommons.org/licenses/by/4.0), which permits unrestricted use, distribution, and reproduction in any medium, provided the original work is properly cited.

Abstract

Maintaining a stable sample position is a critical challenge in optical coherence tomography (OCT), as axial motion can shift the surface outside the imaging range or degrade image quality, particularly at high fringe frequencies with low signal-to-noise ratio (SNR). This work presents an automated motorized reference arm for online surface tracking in OCT. The surface position is extracted from OCT B-scans using an ROI-guided, column-wise infinite impulse response (IIR) edge detection method that directly identifies the air–sample interface from the depth-wise filter response. The detected surface position is used as feedback for a proportional–integral–derivative (PID) controller, which adjusts the reference arm to maintain a predefined axial setpoint. The controller is integrated into a real-time OCT system and evaluated. Results demonstrate stable surface tracking with low residual error and robust step response. This approach enables OCT imaging for dynamic and robotic scanning applications without manual reference arm adjustment.

I. Introduction

Optical coherence tomography (OCT) [1] is a widely used imaging modality that enables non-invasive, high-resolution, depth-resolved visualization of biological tissue and materials. In typical OCT configurations, the usable axial imaging range is limited to a few millimeters in tissue due to coherence length, detection bandwidth, and sensitivity roll-off constraints [2]. Although longer axial ranges can be achieved by reducing the optical bandwidth or increasing detection bandwidth—at the cost of axial resolution—most practical OCT systems operate in a regime where axial range and resolution must be carefully balanced. For instance a swept light source with 100 nm optical bandwidth centered at 1300 nm at a sweep rate of 1.6 MHz achieves an axial imaging range of approx. 5 mm when sampled with 4 GSa/s. A small change in the optical path length difference between the sample surface and the reference arm mirror can cause the sample to move outside the axial imaging range, leading to reduced signal quality or complete signal loss.

This limitation becomes particularly relevant when imaging dynamic in vivo samples or when using hand-held probes, where axial motion cannot be fully avoided. In such scenarios, maintaining a stable optical path length difference is essential for reliable image acquisition. Manual adjustment of the reference arm is insufficient for compensating rapid or unpredictable surface motion, especially without real-time imaging or MHz-OCT [3].

A possible solution to this challenge is the use of an automated motorized reference arm that dynamically compensates for surface displacement, which is only limited by the confocal parameter of the imaging optics. By continuously adjusting the reference arm position based on

10.18416/SCP.2026.2613

© 2026 Infinite Science Publishing

the detected surface location, the sample surface can be maintained within the upper third of the axial imaging range, as this region typically provides higher SNR and more stable image quality.
In this paper, an automated reference arm closed-loop control system for online surface tracking in OCT is presented. The proposed approach extracts the surface position directly from OCT B-scans using a region-of-interest (ROI)–guided, column-wise infinite impulse response (IIR)–based surface edge detection method. The detected surface position is used as feedback for a closed-loop proportional–integral–derivative (PID) controller that adjusts the reference arm position. The system is implemented using a custom real-time OCT software framework and experimentally evaluated under controlled surface motion to demonstrate stable tracking performance and a fast recovery after a step-like deterioration.

II. Methods and Materials

II.I. OCT System and Interferometer Setup

The experimental setup is based on a swept-source system employing a Fourier-domain mode-locked (FDML) laser [4]. The laser operates at a center wavelength of 1300 nm with a sweep bandwidth of approximately 100 nm. An A-scan rate of 1.6 MHz is used, enabling high-speed imaging suitable for fast sample tracking.
Interference signals are detected using a balanced photodiode (PDB480C-AC, Thorlabs Inc., USA) with an analog bandwidth of 1.6 GHz and digitized by a high-speed analog-to-digital converter (ATS9373, Alazar Technologies Inc., Canada) operating at a sampling rate of 4 GSa/s. Data acquisition, OCT signal processing, and visualization are performed using the Lübeck University Real-time OCT (LURO) software [5].
The OCT interferometer is implemented in a fiber-based Mach-Zehnder configuration consisting of a sample arm and a reference arm. The scanning optics are mounted to the end effector of a fully articulated robotic arm (LBR iiwa 14 R820, KUKA AG, Germany) [6].
The reference arm contains a mirror mounted on a motorized linear translation stage, which allows adjustment of the optical path length to compensate axial surface motion.
The OCT volume in the preview mode of the OCT software consists of 2048 A-scans, 16 B-scans, and, according to the sampling rate, 1200 depth voxels. The volume update rate is approximately 50 Hz but can vary due to computational load within ± 5 Hz. A schematic overview of the OCT system and the automated reference arm control loop is shown in Fig. 1.

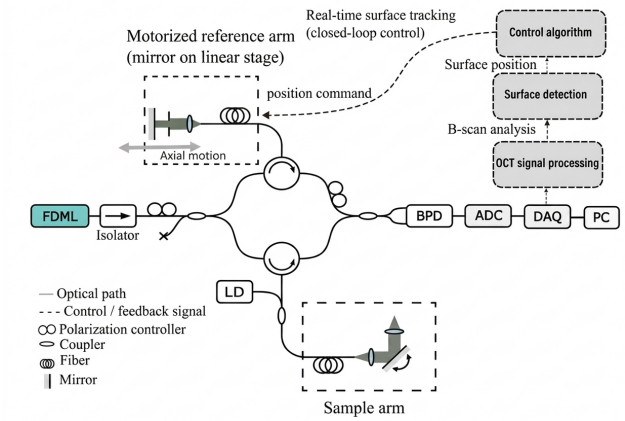


Figure 1: Schematic overview of the OCT system with automated reference arm control. A fiber-based Mach-Zehnder interferometer is used, with a motorized reference arm carrying a mirror on a linear translation stage. Interference signals are detected by a balanced photodiode (BPD), digitized by an analog-to-digital converter (ADC) and data acquisition (DAQ) system, and processed in real time on a PC. Surface detection and feedback control generate position commands to stabilize the surface position.

II.II. Motorized Reference Arm

The reference arm is implemented as a free-space optical path with a mirror mounted on a motorized linear translation stage. Translating the mirror changes the reference arm optical path length and thereby compensates axial sample motion without requiring active modification of the sample arm.
Mirror translation is achieved using a bipolar stepper motor (Nanotec ST3518M1004-A) driven by a TMC2209 microstepping driver. The driver receives step, direction, and enable signals from a microcontroller board (Arduino Mega 2560–compatible, ATmega2560, Elegoo, China), which converts high-level motion commands into smooth mechanical movement. The motor is operated with a microstepping setting of 1/16, which is internally interpolated by the driver to an effective resolution of 1/256 microsteps. This fine step resolution enables smooth and continuous motion of the reference mirror while suppressing mechanical vibration and high-frequency step-induced noise.
The motorized reference arm serves as the actuator of the surface tracking system. For each incoming B-scan, the control system computes a corrective displacement command that is translated into motor steps using a calibrated scale factor. The reference arm motor controller operates in closed loop with the surface detection and feedback control modules.

II.III. Surface Detection and Signal Processing

The surface detection is performed on a single B-scan for each processed volume. Each B-scan is a two-dimensional intensity image where columns correspond to A-scans and rows represent axial sample

10.18416/SCP.2026.2613
© 2026 Infinite Science Publishing

indices. To improve robustness and reduce computational cost, the algorithm first determines a depth region of interest (ROI). For each frame, the intensities are summed laterally across all columns for every depth index, excluding the first ten rows. Skipping the top rows suppresses the constant zero frequency contribution near the top of the image and stabilizes subsequent processing. The depth with the maximum summed intensity is interpreted as the approximate location of the dominant air–sample interface, and the ROI is centered around this depth with a margin of ± 50 pixels.
Within the ROI, surface detection is performed independently for each A-scan using a first-order IIR filter applied along the depth direction. As the algorithm steps through depth indices inside the ROI, the filter state is updated recursively according to Equation (1).

$$y[n] = a\, y[n-1] + b\, x[n] \tag{1}$$

where $x[n]$ denotes the OCT intensity at depth index (n) and $y[n]$ is the filtered response. The coefficient a controls the amount of smoothing along depth, with larger values producing a smoother but slower-responding signal, while b scales the contribution of the current intensity sample. The IIR coefficients were fixed at $a = 0.95$ and $b = 0.05$, satisfying $a + b = 1$.
For each A-scan, the surface position is defined as the first depth index within the ROI at which the filtered response exceeds a predefined threshold. The threshold is selected empirically for each sample to minimize the influence of outliers on the subsequent straight-line fit. Samples with high surface reflectivity require a higher threshold, whereas weakly scattering surfaces can be analyzed using a lower threshold. Once this crossing is detected, processing for that column stops, which avoids unnecessary computation and improves runtime efficiency. The whole surface detection algorithm (auto ROI detection, IIR filtering) takes between 1–2 ms for an entire B-scan of 2048 A-scans allowing a maximum OCT frame rate between 500 Hz and 1000 Hz. Although the stopping depth varies between individual A-scans, the complete B-scan is always processed. The resulting runtime variation is negligible for feedback control, since the total surface detection time of 1–2 ms is substantially shorter than the OCT volume update interval of approximately 20 ms. Columns in which no threshold crossing occurs within the ROI are marked as invalid and are not considered for further processing.
After processing all columns, the detected surface points are combined into a single surface value per B-scan by fitting a straight line to the valid lateral surface locations and evaluating it at the lateral center. This yields one surface height estimate per B-scan for subsequent tracking and control.

II.IV. Feedback Control

The filtered surface position obtained from the signal processing step is used as input to a closed-loop controller that adjusts the reference arm position to compensate axial surface motion by correcting the optical path length. Surface positions are measured in pixel units and converted to physical displacement using a calibrated scaling factor of 189.1 px/mm, enabling a direct relationship between the detected surface position and the commanded mechanical motion. The scaling factor was experimentally calibrated by moving the reference arm between known physical positions and measuring the corresponding surface positions in pixels. Repeated measurements were averaged to improve the accuracy of the calibration, which applies to a refractive index of $n = 1$ (air).
A PID controller is employed to generate relative motion commands for the motorized reference arm. The controller gains are tuned empirically; in the experiments presented here, the proportional and derivative terms are enabled while the integral term is set to zero, with representative values of $K_p = 0.25$, $K_i = 0$, and $K_d = 0.005$. The P gain is selected so that the speed is maximized without causing oscillations around the setpoint. The controller output is applied as a relative position command to the translation stage, providing continuous compensation of surface motion at the system frame rate.

III. Results and Discussion

III.I. Surface Detection Performance

Figure 2 shows the surface detection performance on an OCT B-scan. In Fig. 2(a), the detected surface is overlaid on the full B-scan and accurately follows the air–sample interface across the lateral extent of the scan despite speckle noise. Fig. 2(b) shows a zoomed view near the detected surface, confirming accurate alignment between the detected curve and the surface boundary and that it is not influenced by deeper tissue structures.

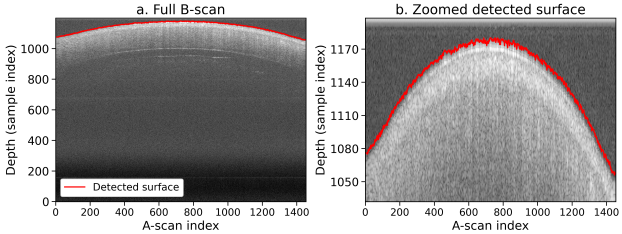


Figure 2: Surface detection results on an OCT B-scan. (a) Full B-scan with the detected surface overlaid in red. (b) Zoomed view of the region near the detected surface, illustrating accurate localization of the surface boundary.

III.II. Closed-Loop Tracking Performance

To evaluate closed-loop reference arm control under controlled axial motion, the fully articulated robotic arm with the mounted OCT scan head was moved in a

10.18416/SCP.2026.2613
© 2026 Infinite Science Publishing

step-like pattern in the axial (z) direction, while the sample remained stationary in the world coordinate system. The sample consists of a flat, highly scattering white paper surface placed under the OCT scanning optics, and the control objective was to maintain the detected surface at a predefined axial setpoint by compensating the imposed motion with the motorized reference arm.

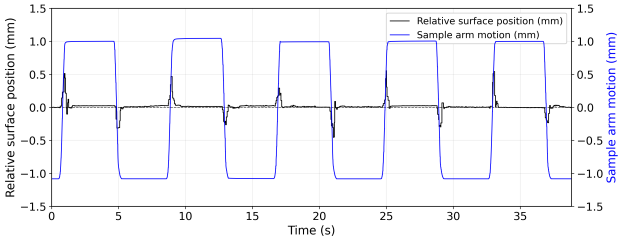


Figure 3: Closed-loop axial tracking during a programmed step-like z-motion of the robotic sample arm over a flat white paper target. The tracking error is shown relative to the surface setpoint (0).

The robot performed 10 successive axial steps of ±1 mm relative to the setpoint. The resulting tracking error and sample arm motion are shown in Fig. 3. Between step transitions, the tracking error remains close to zero, indicating stable surface localization, while brief transients occur at each step before the controller restores the surface position.
Figure 4 shows zoomed views of two representative step responses. Fig. 4(a) illustrates a negative step (from the upper to the lower position), while Fig. 4(b) shows a positive step (from the lower to the upper position). The measured displacement is approximately 2.1 mm in both cases, slightly exceeding the nominal 2.0 mm command due to the finite positioning and repetition accuracy of the robotic system.

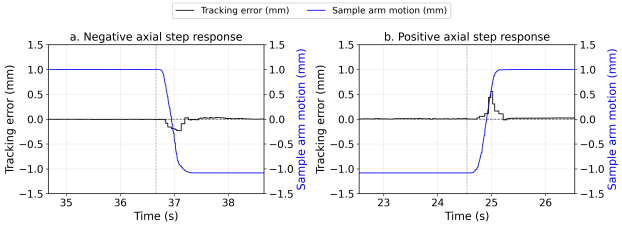


Figure 4: Two representative closed-loop step responses: (a) negative axial step and (b) positive axial step. In both cases the reference arm compensates the displacement and returns the surface position toward the setpoint.

For the negative step in Fig. 4(a), a displacement of approximately 2.1 mm results in a peak tracking error of about 0.23 mm (11%), which returns to within ±50 μm of zero in approximately 0.54 s. For the positive step in Fig. 4(b), a similar displacement (≈ 2.1 mm) produces a larger peak tracking error of about 0.56 mm (27%) with a longer transient. In both cases, the tracking error converges back toward zero without sustained deviation, demonstrating stable closed-loop behavior.

The step-like motion used here does not represent typical real-world sample motion but serves as a controlled stress test. The results show that the reference arm can compensate rapid axial motion, indicating suitability for slower and more continuous motion such as gradual drift or tremor-like movement in OCT imaging.

The proposed approach has two main limitations. Reference arm compensation is only meaningful while the sample remains within the confocal parameter (depth of focus) of the OCT scanning optics, as large axial shifts can move the surface outside the region of optimal focus and degrade image quality. The method was evaluated on flat sample surfaces using a straight-line fit and a single central surface value for control; tilted or strongly curved surfaces would require alternative surface metrics or spatially resolved control strategies. Despite these constraints, the system provides reliable and fast axial surface stabilization.

IV. Conclusion

An automated reference arm for online surface tracking in OCT was presented. The method relies on ROI-restricted surface detection combined with IIR filtering to obtain a stable, surface position estimate suitable for closed-loop control. This enables reliable axial surface stabilization during OCT imaging under motion, making the approach well suited for real-time and dynamic measurement scenarios.

Acknowledgments

The work has been carried out and supervised by the Institute of Biomedical Optics, Universität zu Lübeck.

Author's statement

Conflict of interest: Authors state no conflict of interest.

References

[1] D. Huang *et al.* Optical coherence tomography. *Science*, 254(5035):1178–1181, 1991, doi:10.1126/science.1957169.

[2] S. Lotz and R. Huber. Superior dynamic range roll-off in a mhz fourier domain mode-locked laser by a high-finesse fabry–pérot filter. *Optics Letters*, 50(17):5310–5313, 2025, doi:10.1364/OL.567200.

[3] W. Wieser *et al.* Multi-megahertz oct: High quality 3d imaging at 20 million a-scans and 4.5 gvoxels per second. *Optics Express*, 18(14):14685–14704, 2010, doi:10.1364/OE.18.014685.

[4] R. Huber *et al.* Fourier domain mode locked lasers for swept source optical coherence tomography. *Optics Express*, 14(8):3225–3237, 2006, doi:10.1364/OE.14.003225.

[5] W. Draxinger *et al.* Microscope integrated mhz optical coherence tomography system for neurosurgery: Development and clinical in-vivo imaging. *Biomedical Optics Express*, 15(10):5960–5977, 2024, doi:10.1364/BOE.532477.

[6] S. Lotz *et al.* Large area robotically assisted optical coherence tomography (lara-oct). *Biomedical Optics Express*, 15(6):3993–4009, 2024, doi:10.1364/BOE.525524.

© 2026 Infinite Science Publishing